IChemE

www.icheme.org/journals
doi: 10.1205/cherd.03394

0263–8762/05/$30.00+0.00

Trans IChemE, Part A, January 2005
Chemical Engineering Research and Design, 83(A1): 40–49

COMPUTATIONAL FLUID DYNAMICS SIMULATIONS OF TAYLOR BUBBLES IN TUBULAR MEMBRANES
Model Validation and Application to Laminar Flow Systems

N. V. NDINISA[1], D. E. WILEY[1] and D. F. FLETCHER[2,*]

[1]*UNESCO Centre for Membrane Science and Technology, University of New South Wales, NSW, Australia*
[2]*Department of Chemical Engineering, University of Sydney, NSW, Australia*

The use of gas–liquid two-phase flow has been shown to significantly enhance the performance of some membrane processes by reducing concentration polarization and fouling. However, the understanding of the mechanisms behind gas–liquid two-phase flow enhancement of flux is still limited. This paper reports on the validation of computational fluid dynamics simulations of a Taylor bubble, using a variety of numerical approaches. Good agreement between the experimental and numerical data is shown for an Eulerian two-fluid model that uses a solution adaptive bubble size to avoid numerical mixing. This model is then used to study the effect of liquid extraction at the membrane wall on the wall shear stress, since it is the enhanced wall shear stress caused by the bubble passage that is important. This effect is shown to be negligible for typical operating conditions in membrane systems. Moreover, we show that the wall shear stress can be well represented by a 'top hat' profile for the system considered here.

Keywords: Taylor bubble; CFD; model validation; tubular membrane; wall extraction.

INTRODUCTION

The use of gas sparging through tubular membranes is increasing in importance because of its ability to reduce fouling and/or reduce concentration polarization effects (Cui *et al.*, 2003). Several researchers have evaluated the effect of bubbling on the performance of membrane filtration by injection of air into the lumen of tubular and hollow fibre membranes. These studies include ultrafiltration of dextran with tubular membranes (5 mm i.d.) and hollow fibres (0.2 mm i.d.; Cui and Wright, 1996; Bellara *et al.*, 1996); filtration of bentonite suspension with tubular membranes (15 mm i.d.) and hollow fibres (0.93 mm i.d.; Cabassud *et al.*, 1997; Mercier *et al.*, 1997); ultrafiltration and microfiltration of yeast suspensions using 15 and 6 mm i.d. tubular membranes (Mercier *et al.*, 1998); and ultrafiltration and microfiltration of bacterial suspensions using flat sheet membranes (Lee *et al.*, 1993). All of these experiments show that air injection can result in an improvement in flux but the extent of the enhancement depends on the type of module (tubular or hollow fibre) and the membrane type. For tubular membranes, the enhancement was about two to three-fold, while for hollow fibres the gain was 1.0–1.3. The effect of air slugs on flux was more pronounced with ultrafiltration membranes than with microfiltration membranes (Mercier *et al.*, 1998; Lee *et al.*, 1993).

Crossflow microfiltration in tubular membranes is often carried out under turbulent flow regimes in order to minimize concentration polarization and fouling. This usually requires high cross-flow velocities, which inevitably lead to high energy consumption. The use of two phase flow lowers the required velocities, allowing systems to be operated under laminar flow conditions. However, the introduction of gas causes the transition from laminar to turbulent flow to occur much faster (Ghosh and Cui, 1999). Several researchers have investigated the effectiveness of two-phase flow under laminar and turbulent flow conditions in tubular membrane modules (Cui and Wright, 1996; Cabassud *et al.*, 1997; Vera *et al.*, 2000; Taha and Cui, 2002). All of these researchers found that the flux enhancement by two-phase flow decreased as the Reynolds number was increased. For example, Cui and Taha (2003) found a flux enhancement of 160% with a Reynolds number of 490, whilst at a Reynolds number of 3150 the flux enhancement was only 5%. These studies therefore suggest that it is optimal to operate two-phase flow in the laminar regime.

*Correspondence to: Dr D. F. Fletcher, Department of Chemical Engineering, University of Sydney, NSW 2006, Australia.
E-mail: davidf@chem.eng.usyd.edu.au

It is believed that the enhanced wall shear stress created as the liquid flow is squeezed past the bubble is the primary enhancement mechanism, as it removes foulants from the walls. Wall shear stress profiles around Taylor bubbles have been determined using electrochemical methods for systems with a non-porous wall in place of a membrane (Cabassud *et al.*, 2001; Mercier-Bonin *et al.*, 2000; Ducom *et al.*, 2002). Taha and Cui (2002) have used computational fluid dynamics (CFD) to predict the wall shear stress profile of a Taylor bubble in a 10 mm tube without extraction (see below for more details). They then used the predicted shear stress to calculate mass transfer and hence permeate flux for a tubular membrane of the same diameter. However, in their CFD simulation they used a non-porous tube and so the predicted shear stresses did not account for the porous wall.

Wang *et al.* (1994) cite Howell *et al.* (1992) as concluding that in their experiments wall suction of up to 1% of the inlet flow did not distort the macroscopic flow field. The paper by Howell *et al.* (1992) reports CFD simulations of flow patterns and particle motion which occur during oscillatory flow in a baffled channel with and without porous walls. They conclude that 'There is not much effect of 1% wall flux on flow patterns except near the wall region', but as their system is very different from the present one and no details of the modelling are given, their work cannot be used to justify the assumption that in general extraction has no effect on bubbling flows.

Therefore the main objective of this study is to validate a CFD model of Taylor bubble flow in a tubular column and to examine what effect wall flux has on the liquid flow field. The numerical model was validated using experimental data obtained by Bugg and Saad (2002) using particle image velocimetry (PIV) for a bubble rising in a stagnant liquid. Then wall suction rates as high as 20% of the flow extracted over 16 tube diameter lengths have been investigated. For membranes, the flux is typically 15% of the flow extracted over a length of more than 250 tube diameters (Wang *et al.*, 1994), so the current results more than cover the entire practical range of operation.

PREVIOUS WORK ON TAYLOR BUBBLE SIMULATION

Before describing the modelling work it is important to cite White and Beardmore (1962), who conducted a series of experiments on Taylor bubbles rising in stagnant liquids in vertical tubes. Their work is used extensively in model validation, and they determined the important dimensionless groups to characterize Taylor bubbles. They identified the Eötvös number ($\rho g D^2/\sigma$), the Froude number (U_t^2/gD) and the Morton number ($g\mu^4/\rho\sigma^3$) as the important dimensionless groups. In these groups U_t is the terminal speed of the bubble, g is the acceleration due to gravity, D is the tube diameter, ρ is the liquid density, σ is the surface tension, and μ is the dynamic viscosity of the liquid. Other dimensionless groups which have been used are the Weber number ($\rho U_t^2 d_b/\sigma$) and the bubble Reynolds number ($\rho U_t d_b/\mu$), where d_b is the equivalent diameter of the bubble. Combining their work with the work of others, White and Beardmore (1962) produced a comprehensive graphical correlation of Froude number as a function of the Eötvös and Morton numbers. They concluded that viscous forces are negligible if $\rho^2 g D^3/\mu^2 > 3 \times 10^5$, interfacial forces are negligible if $Eo > 70$, and inertial effects are negligible if $Fr < 0.05$.

Slug flow is encountered in many industrial applications. It occurs in hydrocarbon production and transportation, chemical and nuclear reactors, and phase change heat transfer. Two-phase flow has also been shown to enhance heat and mass transfer coefficients. Although slug flow has been widely studied experimentally, simulation of two-phase flow is a relatively new subject. The first computer codes for the simulation of two-phase flow were pioneered by the nuclear industry and adopted as a primary tool for simulating possible loss of coolant accidents in nuclear reactors. These codes have been modified for use in the oil industry to simulate transient two-phase flow in pipelines (Taitel *et al.*, 1989). Tomiyama *et al.* (1993) were amongst the first to study bubble behaviour using VOF methods and showed that this technique produced qualitatively correct bubble shapes for a variety of conditions. They also studied the effect of an imposed shear field on the bubble trajectory and the dependence of this trajectory on the bubble and fluid properties.

There are many hydrodynamic models which have been developed to study slug flow but most of them have not been validated experimentally. Kawaji *et al.* (1997) were among the first to validate numerical simulations of slug flow with experimental data. The RIPPLE code that uses a VOF interface tracking method was used to simulate the hydrodynamics of a Taylor bubble rising through stagnant liquid in a vertical tube. The simulation was performed in a frame of reference moving with the bubble, so that the liquid and the tube wall moved downward at the bubble terminal velocity. The simulations were axisymmetric, transient and two-dimensional. Bubbles of different lengths were simulated and the terminal speed was found to be the same for all bubbles. The *Eo* and *Mo* numbers in their simulations were 232 and 3.06×10^{-9}, respectively. According to the graphical correlation of White and Beardmore (1962), the bubble hydrodynamics in this region is independent of viscous and interfacial forces and is inertia-dominated. The flow in the falling film was found to be laminar and for shorter bubbles it penetrated deeper into the wake than for longer bubbles. The VOF model underpredicted the wall shear stress and velocity near the tube wall, while the differences diminished towards the interface. Based on the simulations, they conjectured that the residual eddies far below the wake of the leading bubble cause perturbations in the pressure and liquid flow field that in turn cause the trailing bubble to move laterally or deform its shape, which can lead to reduced drag force and an increase in the rise velocity.

Bugg *et al.* (1998) investigated the motion of bubbles in tubes using a two-dimensional, transient, finite difference model with volume fraction specification to track the movement of the gas–liquid interface. The simulations were axisymmetric and used a fixed frame of reference. Taylor bubbles rising through a stagnant liquid in a vertical tube were simulated for a wide range of Eötvös numbers between 10 and 100, and Morton numbers between 10^{-12} and 10. The main purpose of their investigation was to predict the final steady-state shape of the bubble for various flow profiles around the Taylor bubble. For all conditions, the initial shape of the bubble was the same but the final shape differed depending on whether viscous or inertial

forces were important. All the simulated bubbles had the expected spherical nose and the trailing edge had a flat or rounded shape depending on the Froude number (*Fr*). For all cases with $Fr > 0.3$, it was observed that the bubbles had flat or concave bottoms. This was seen to be a better criterion for predicting the bubble shape at the bottom compared with earlier criteria proposed by White and Beardmore (1962) and Fabre and Liné (1992). For the cases in which viscous forces were unimportant, based on the White and Beardmore (1962) criterion, it was found that the falling film continues to thin all the way to the trailing edge of the bubble. In the cases where viscous effects were important, a portion of the falling film had a constant thickness, indicating that the falling film had reached equilibrium.

The numerical code used by Bugg *et al.* (1998) was recently validated against experimental data by Bugg and Saad (2002). The code uses a VOF method to track the gas liquid interface. In the experiments, a Taylor bubble rising through olive oil in a 19 mm i.d. tube was investigated. In this simulation the Eötvös number was 100 and the Morton number was 0.015. Experimental data were obtained using the PIV technique. PIV measurements were validated by using a mass balance equation to calculate the terminal velocity of the bubble. The resulting terminal velocity was within 3% of the terminal velocity measured using the phase transition detectors. The terminal velocity predicted by the numerical method was within 7% of the experimental value. Velocity profiles were measured for the region ahead of the bubble, in the developing film, in the fully developed film, as well as in the wake region. There was excellent agreement between experimental and numerical velocity profiles in all regions, except in the wake region where the maximum axial velocity was under-predicted by about 15%. This was attributed to the fact that the bottom edge of the bubble is not as rounded in the predictions as in the experiments.

Mao and Dukler (1991) developed a numerical model of the flow around a Taylor bubble using a curvilinear coordinate system attached to the bubble and fitted to the bubble shape. No *a priori* assumptions were made about the shape of the gas bubble. The model adjusted the shape of the interface so that normal stress at the interface satisfied the condition of constant pressure inside the bubble. The simulations were transient, axisymmetric and two-dimensional using a frame of reference moving with the bubble. The terminal velocity of the bubble was adjusted until the bubble was locally spherical at the nose. The solution domain extended only to the trailing edge of the bubble and not into the wake region. A modified RNG $k-\varepsilon$ turbulence model was used when the liquid flow was turbulent. The computed Froude number was 0.346, which is very close to the experimental value of 0.351. The terminal velocity was found to be independent of viscosity and surface tension. The predicted wall shear stress increased along the side of the bubble and showed a wavy pattern towards the bottom, reflecting a wavy interface.

Clarke and Issa (1997) used a finite volume computational procedure to analyse the liquid flow field around a Taylor bubble rising in a vertical tube. A non-orthogonal block structured mesh which can map the entire flow field around the Taylor bubble and in the liquid slug behind it was used. The flow inside the bubble was ignored. Turbulence was modelled using the standard $k-\varepsilon$ model. The rise velocity of the bubble was determined by a trial-and-error method, with the final correct velocity producing a bubble nose which is locally spherical at the stagnation point. Although the model calculated the shape of the bubble, the bottom part of the bubble was assumed to be flat. The simulations were two-dimensional axisymmetric and used a frame of reference moving with the bubble. This model also accounts for the presence of small dispersed bubbles in the liquid slugs by assuming homogeneous two-phase flow in this region. However, the homogeneous model was found to be inadequate in resolving two-phase flow in the liquid slug and hence the authors indicated that future models need to use the two-fluid model in order to account for dispersed bubbles correctly.

Issa and Ubbink (1999) developed a new algorithm for solving the volume fraction equation to preserve a sharp interface between the two fluids and applied this to Taylor bubble simulations. The interesting feature of this algorithm is that the advection scheme was constructed to have minimal numerical diffusion without dispersive errors by making the convection scheme depend on the flow orientation relative to the cell face in the discretized equations. They carried out an extensive series of simulations to determine the bubble rise velocity for a variety of Eötvös and Morton numbers and obtained good agreement with the data of White and Beardmore (1962), except in cases where the surface tension force was dominant.

As discussed in the Introduction, slug flow has been shown to enhance the performance of membrane systems. In an attempt to understand the flux enhancing mechanisms of slug flow Taha and Cui (2002) used a VOF method to model slug flow in a tubular ultrafiltration (UF) process. The model was used to calculate the shape and velocity of the slug, as well as the velocity distribution and local wall shear stress at the membrane surface. The predicted wall shear stress was then linked to the local mass transfer coefficient that was used to predict the permeate flux. The commercial CFD code FLUENT was used for the simulations which were transient, two-dimensional and axisymmetric, with a frame of reference moving with the bubble being used. The RNG $k-\varepsilon$ turbulence model was used. The shape of the Taylor bubble was predicted with reasonable accuracy. The predicted terminal rise velocity of the bubble in a 10 mm i.d. tube was $0.0692\ \mathrm{m\ s^{-1}}$, which is very close to the experimental value of $0.068\ \mathrm{m\ s^{-1}}$.

It is apparent from the review of numerical methods that almost all the codes used have been specifically created for the simulation of slug flow, with the exception of that of Taha and Cui (2002), who used the general purpose, commercial CFD code FLUENT. However, Taha and Cui did not present velocity profile distributions around the Taylor bubble and their method of validation was indirect. Bugg and Saad (2002) conducted an excellent validation of their numerical model for the case of slug flow but they used a purpose written code specifically developed for this application. It is also clear from the literature that most researchers have used a frame of reference moving with the bubble which is less complicated than simulating a bubble rising from rest, but requires the terminal velocity of the bubble to be known *a priori* or to be adjusted

iteratively. Therefore the aim of this paper is to study various two-phase flow models available in a general purpose commercial CFD code, CFX 5.6. The simulations are also conducted in a manner that closely resembles experimental conditions, in that a bubble is allowed to rise from rest.

THE NUMERICAL SOLUTION METHOD

In this section the various approaches used here to model two phase flow are presented and their application to this problem is described.

The Euler Two-fluid Model

In this approach, the fluids are treated as two interpenetrating continua, each having their own velocity field, each occupying separate regions in space but sharing a common pressure field. The two-fluid model is best suited for situations where there is a continuous and a disperse phase where the continuous/disperse phase interface is smaller than the grid-size. However, use of appropriate closure correlations also allows for the simulations of two-phase flow phenomena where the characteristic length of the interface is large compared with the grid size. The interaction between the fluids is through the shared pressure field, the exchange of momentum via interfacial drag and other forces. Both fluids share space in proportion to their volume fractions which satisfy the condition

$$\alpha_G + \alpha_L = 1 \tag{1}$$

The two-fluid model is developed by writing conservation equations for each phase separately. Through the use of appropriate averaging techniques, these conservation equations can be used to represent macroscopic flow fields for each phase. However, during the process of averaging, important characteristics of the flow fields are lost and must be reintroduced into the model via appropriate closure laws. For isothermal two-phase laminar flow, the governing conservation equations are:

$$\frac{\partial \rho_k \alpha_k}{\partial t} + \nabla \cdot (\rho_k \mathbf{u}_k \alpha_k) = 0 \tag{2}$$

$$\frac{\partial \alpha_k \rho_k \mathbf{u}_k}{\partial t} + \nabla \cdot (\alpha_k \rho_k \mathbf{u}_k \otimes \mathbf{u}_k) = -\alpha_k \nabla p + \nabla \cdot \alpha_k \boldsymbol{\tau}_k + \sum_{l=1}^{N} \mathbf{M}_{kl} + \alpha_k \rho_k \mathbf{g} \tag{3}$$

where ρ_k, $\mathbf{u}_k$, α_k and $\boldsymbol{\tau}_k$ are the macroscopic density, the velocity, the volume fraction and the viscous stress tensor of the kth phase. p is the pressure and $\mathbf{M}_{kl}$ is the interphase momentum exchange term between phase k and phase l. The important term that requires modeling is $\mathbf{M}_{cd}$ which for a continuous phase c and a disperse phase d takes the form:

$$\mathbf{M}_{cd} = \frac{(3/4)\alpha_d c_d \rho_c |\mathbf{u}_d - \mathbf{u}_c|(\mathbf{u}_d - \mathbf{u}_c)}{d_d} \tag{4}$$

where c_d is the drag coefficient (set to 0.44 here), ρ_c is the density of the continuous phase and d_d is the disperse phase length-scale. As we will see later, the behaviour of the system of equations can be changed significantly by manipulating the disperse phase length-scale.

The Volume-of-fluid Model

The volume-of-fluid (VOF) model is suitable for describing two-phase problems where the characteristic length scale of the interface is larger than the grid size. The VOF method, originally developed by Hirt and Nichols (1981), tracks the motion of the gas–liquid interface and accounts for topological changes in the interface by using a transport equation for f, the fraction of space occupied by the liquid phase. The governing mass and momentum equations are derived from the two-fluid model by assuming no slip between the phases and that all properties are volume fraction weighted averages, giving

$$\frac{\partial \rho}{\partial t} + \nabla \cdot (\rho \mathbf{u}) = 0 \tag{5}$$

$$\frac{\partial \rho \mathbf{u}}{\partial t} + \nabla \cdot (\rho \mathbf{u} \otimes \mathbf{u}) = -\nabla p + \nabla \cdot \boldsymbol{\tau}_k + \rho \mathbf{g} + \mathbf{F}_{SF} \tag{6}$$

where the fluid properties are function of space and time and are given by

$$\rho(\mathbf{x}, t) = f(\mathbf{x}, t)\rho_L + [1 - f(\mathbf{x}, t)]\rho_G \tag{7}$$

$$\mu(\mathbf{x}, t) = f(\mathbf{x}, t)\mu_L + [1 - f(\mathbf{x}, t)]\mu_G \tag{8}$$

The subscripts L and G indicate the liquid and gas phases, respectively. The model solves the scalar advection equation for one of the volume fractions, f, via

$$\frac{\partial f}{\partial t} + \nabla \cdot (\mathbf{u} f) = 0 \tag{9}$$

with the other being determined using equation (1).

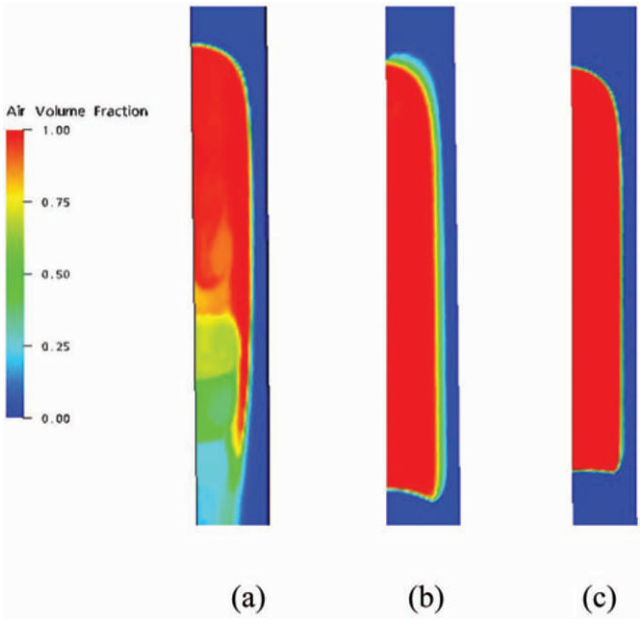

Figure 1. The bubble shape at the end of the simulation for (a) the VOF model, (b) the two-fluid model using a constant disperse phase length-scale of 5 mm, and (c) the combined model in which the disperse phase length-scale was adapted by the solution.

In its simplest form, the VOF method relies on the use of a fine mesh and high order numerical schemes (see Issa and Ubbink, (1999), for an example of this approach) to resolve the interface over a distance of several cells. More sophisticated methods introduce algebraic reconstruction schemes after each timestep, as discussed in for example Harvie and Fletcher (2000).

Finally, surface tension effects need to be included in the above models. The continuum surface force (CSF) of Brackbill *et al.* (1992) is used to model the force due to surface tension ($\mathbf{F}_{SF}$) acting on the gas–liquid interface.

Simulation Conditions

The governing equations for both models were solved using the commercial CFD code CFX 5.6 from ANSYS. This code solves the equations on an arbitrary grid using a finite volume method and a coupled solver. In this study, a two-dimensional structured grid was used. The fluids were assumed to be incompressible and isothermal and to have constant fluid properties. Transient simulations assuming laminar flow in a two-dimensional wedge, representing the vertical tube used experimentally, were performed. The simulations were based on the experimental conditions of Bugg and Saad (2002). The fluid density was set to 911 kg m^{-3}, the viscosity was 0.084 Pa s and the surface tension was 0.0328 N m^{-1}. These chosen fluid properties and tube diameter yield the following dimensionless numbers: $Eo = 100$, $Mo = 0.015$ and $Re = 27$. The regime map of White and Beardmore indicates that for the simulations conducted here the surface tension forces are unimportant.

The tube diameter was 19 mm and the tube height was 160 mm. The tube was modelled as a closed system with walls on the top and the bottom. The initial shape of the bubble was assumed to be cylindrical, with a height of 50 mm and a diameter of 14 mm, located centrally in the tube at 5 mm above the bottom wall. The bubble rises from rest and develops an invariant shape. For the VOF method, a no-slip boundary condition was applied to the walls, whilst in the two-fluid model, the wall boundary conditions were no-slip for the liquid and free-slip for the air.

Mesh variation studies showed that a grid size of 0.25 mm in the radial and 0.25 mm in the axial direction gave grid independent solutions. A constant time step of 0.0001 s was used for all models. Note that both the spatial resolution and the temporal resolution need to be very fine to generate a properly converged solution, independent of the numerical solution parameters.

The VOF model is the classical method of solving a free surface problem. In CFX5.6 this method makes use of second-order numerical schemes for both space and time with a compressive scheme (for both space and time) being applied to the volume fraction (f) equation in order to reduce numerical diffusion to a minimum. No surface reconstruction scheme is used to sharpen the interface.

In the simulations performed using the Eulerian two fluid model, slip is allowed between the two phases. This only affects the solution in computational cells where there is a fluid mixture. Initially, the disperse phase length-scale, (d_d) was set to 5 mm to allow significant slip between the gas and the liquid. This size was chosen on the basis of trial and error, and was found to give the solution the desirable property that cells containing a mixture of gas and liquid would tend to separate. This was needed because significant mixing of the gas and liquid occurred in the wake region in the VOF simulations (see later), most likely because of the difficulty of choosing a physically acceptable set of initial conditions from which to start the simulation. However it has the undesirable effect of thickening the interface in regions where the gas is below the liquid, i.e. at the leading edge of the bubble, and increasing the computational time considerably.

To combat the loss of a sharp interface, a combined model was developed using a variable bubble size. A small bubble size (0.1 mm) was used throughout the domain except in cells where there was a mixture of gas and liquid, and the gas volume fraction gradient was in the opposite direction to gravity. In these cells, a gas bubble size of 5 mm was used, again to allow the gas to rise and rejoin the main bubble. This combined model then behaves like the VOF model (as $d_d = 0.1$ mm gives a very low slip velocity) except in regions where gas and liquid are mixed with liquid above gas, where the high slip velocity means that it behaves like the two fluid model, and the 'gas bubbles' rise to rejoin the bulk of the gas.

MODEL VALIDATION

The bubble shape

The total simulated time for all the models was around 0.95 s, which was sufficient to allow the bubble to reach its terminal velocity. Figure 1 shows air volume fraction plots of the bubble at the end of the simulation for the three models. In the VOF case, the bubble has a sharp interface at the top but a badly mixed wake. The two fluid model with a constant disperse phase length-scale of 5 mm gives a well-defined wake but a much more diffuse interface. Finally, the combined model has the best properties of both simulations. The figure shows a bubble with a prolate spheroidal leading edge and concave trailing edge. For the chosen conditions inertial forces dominate and Fabre and Liné (1992) state that in this regime bubbles have flat or concave bottoms, as observed here. Therefore, the shape predicted by the two-fluid models is qualitatively correct. This shape also matches reasonably well with that observed experimentally by Bugg and Saad (2002).

The terminal velocity

For the VOF model the terminal speed of the bubble was found to be 0.140 m s^{-1}, for the two-fluid model it was 0.119 m/s^{-1} and for combined model it was 0.110 m/s^{-1}. The experimental value of the terminal velocity was 0.131 m/s^{-1} (Bugg and Saad, 2002). The predicted values are within 8% of the experimental value which is comparable with the agreement achieved by Bugg and Saad (2002). Note that the terminal velocity has to be estimated from the movement of the slightly smeared interface and so its value is subject to some uncertainty. This affects subsequent comparisons where all velocities are normalized by the calculated terminal velocity but the effect is judged to be no more than 10%.

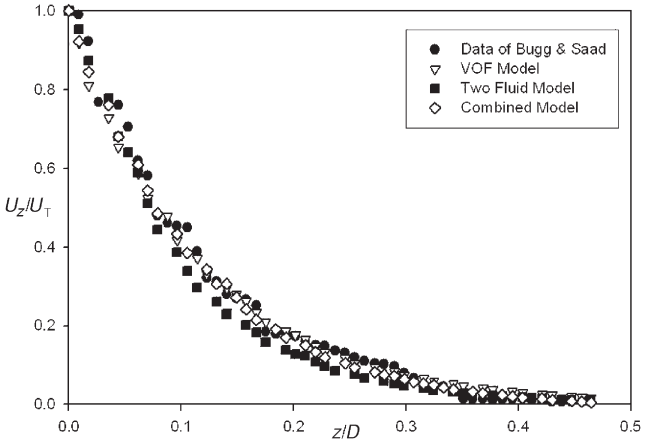

Figure 2. The normalized axial component of velocity along the tube axis above the bubble nose.

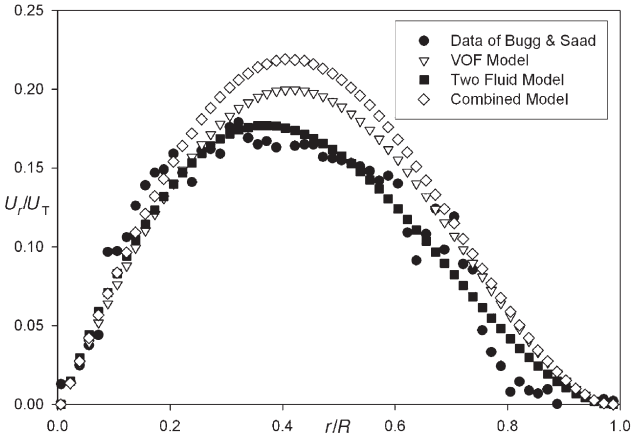

Figure 4. The radial velocity distribution across the tube 0.111*D* above the bubble nose.

Axial velocities along the tube axis

As the bubble rises in the stagnant liquid, it accelerates the fluid ahead of it and this fluid is pushed sideways to allow the bubble to rise. Axial velocities ahead of the bubble were extracted along the tube axis from the bubble nose up to a distance of about 0.5*D*. The velocities from the three models, together with experimental data, are shown in Figure 2. This figure shows that the bubble does not have much influence on the liquid ahead of it, as the axial velocity decays to zero at about 0.3*D*. There is very good agreement between the numerical and the experimental data in all cases.

Axial and radial velocity profiles ahead of the bubble

As the bubble moves upwards, fluid ahead of it is pushed sideways (see Figure 3). As a result, a strong radial velocity component can be seen ahead of the bubble pushing fluid away from the tube axis. Velocity field data are available from the experimental study at a plane located 0.111*D* ahead of the bubble. The point of maximum radial velocity, as seen in Figure 4, is located halfway between the tube wall and the gas–liquid interface. For the axial velocities (shown in Figure 5), initially the fluid moves in an upward direction, but at a distance of about 0.66*D* from the tube axis, the flow changes direction from upward to downward. The transition from upward to downward flow is smooth. For the axial velocities, the agreement between numerical and experimental results is very good for all models. However, for the radial velocities all models seem to over-predict the radial velocities near to the wall. The experimental data suggest that, at about 0.8*D*, the radial velocity decays to zero but this is not in agreement with the numerical methods which show a much smoother and more physically intuitive behaviour. Given the observable scatter in the experimental data, this is most likely explained by measurement difficulties near the wall. The two-fluid model is closer to the experimental results than the VOF model. The combined model also seems to over-predict the peak radial velocity, but near the tube axis and the tube wall it predicted the velocities with reasonable accuracy.

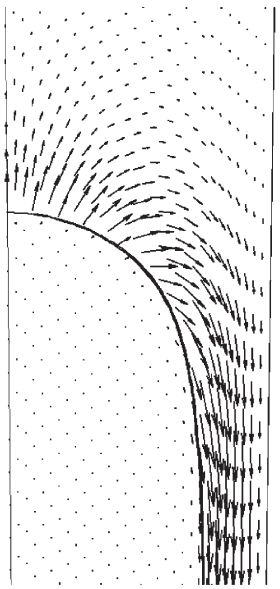

Figure 3. The velocity profile near the Taylor bubble nose. (Vectors are shown at only one-fifth of the computational nodes for clarity.)

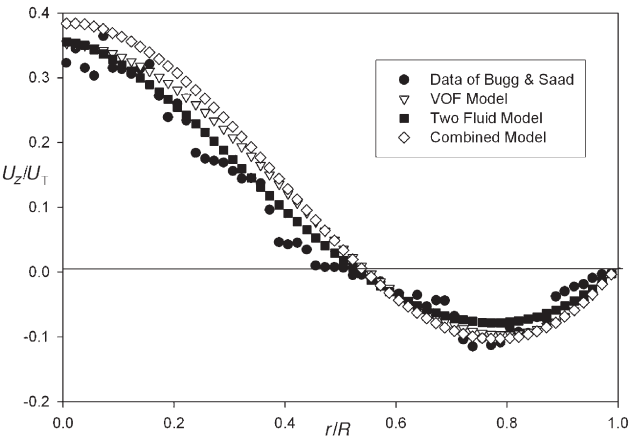

Figure 5. The axial velocity distribution across the tube 0.111*D* above the bubble nose.

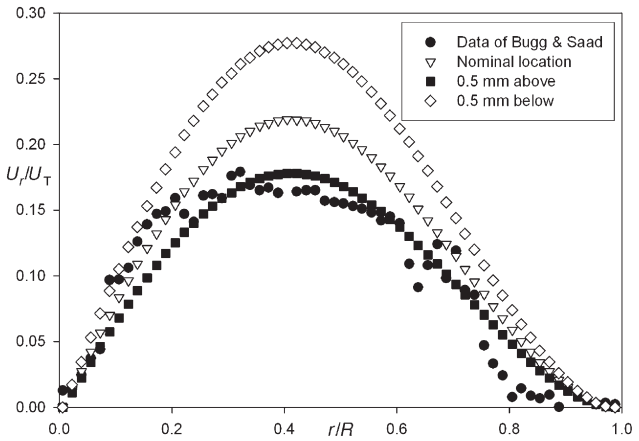

Figure 6. The effect of the sampling location on the radial velocity profile at a distance 0.111*D* above the bubble nose.

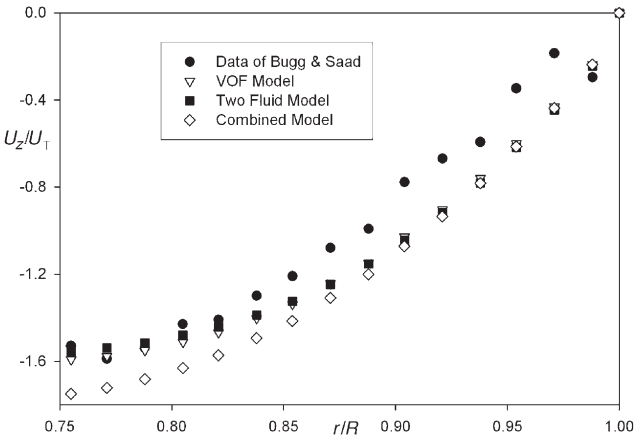

Figure 8. The axial velocity distribution in the developing film at a distance 0.504*D* below the bubble nose.

An interesting feature of the above results in the apparent significant variation of the model results at nominally the same position in the flow. The data are extracted at a fixed location relative to the nose of the bubble, but as has already been noted there is some uncertainty in the exact location of this point. It is clear from Figure 3 that the velocity field is changing rapidly near this location. Therefore, in Figure 6, the data of Bugg and Saad for the radial velocity are compared with results from the combined model at the nominal location and at locations 0.5 mm above and below this location. It is evident that this very small change in location has a relatively large effect on the predicted values and that the observed disagreement between the predictions and the data can easily be explained in terms of the uncertainty of locating the exact same location relative to the bubble nose. Recall that 0.5 mm is just two numerical cell widths, which again highlights the need for very fine numerical meshes to properly resolve the flowfield.

Flow profile in a developing film

In the developing film, near the bubble nose, the radial velocity is quite strong, particularly near the gas–liquid interface, as the bubble pushes the liquid. The maximum radial velocity occurs near the liquid interface. At a point 0.504*D* below the bubble nose the radial velocities are reduced drastically as the fluid accelerates further and the developing film becomes thinner, as can be seen in Figure 7. On the other hand, the axial velocities become stronger and are high near the interface, as seen in Figure 8. The agreement between experimental and numerical results is good for both the radial and axial velocities.

Axial velocity in the fully developed film

The developing film accelerates and thins as it falls, until the shear stress at the wall is capable of supporting the weight of the film and a fully developed film is formed. The radial velocity in the film is then zero and the axial velocity profile no longer changes. Figure 9 shows the velocity profile across the fully developed film, from which it can be seen that the liquid near the gas–liquid interface moves faster than the liquid near the wall due to the negligible shear stress at the gas–liquid interface. The maximum axial velocity in the falling film is more than twice that of the bubble terminal velocity. Figure 8 shows excellent agreement between the results from all three numerical models and the experimental data, although

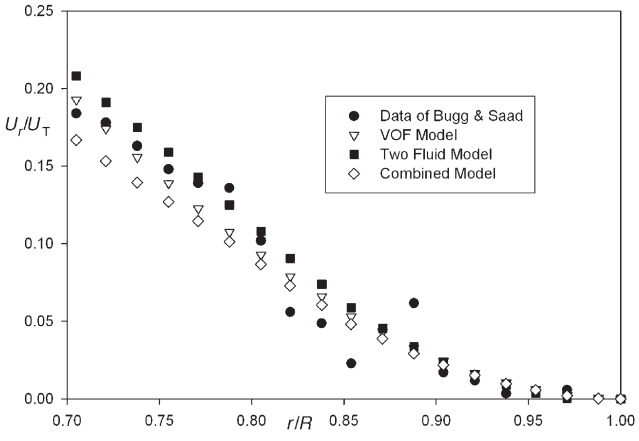

Figure 7. The radial velocity distribution in a developing film at a distance 0.504*D* below the bubble nose.

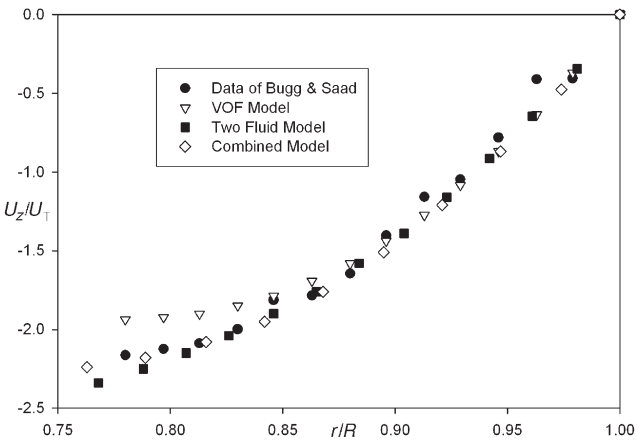

Figure 9. The axial velocity profiles in the fully developed falling film.

the VOF results start to deviate close to the bubble interface because of the artificial mixing present in the wake region (see Figure 1a).

Flow profile in the wake

Owing to the interface mixing problem in the VOF model described earlier, only results from the two-fluid model and the combined model are presented for this region. The rapid change of flow direction in the wake region is shown in Figure 10. The axial velocities reduce dramatically compared with those in the falling film as the fluid changes direction and recirculation occurs in the wake. There is a strong radial velocity component in the wake region, which transfers fluid from the tube wall towards the axis. Radial velocities decay quickly to zero near the tube axis. The axial and radial velocities in the bubble wake are shown in Figures 11 and 12. The agreement between the experimental and numerical results is again very good.

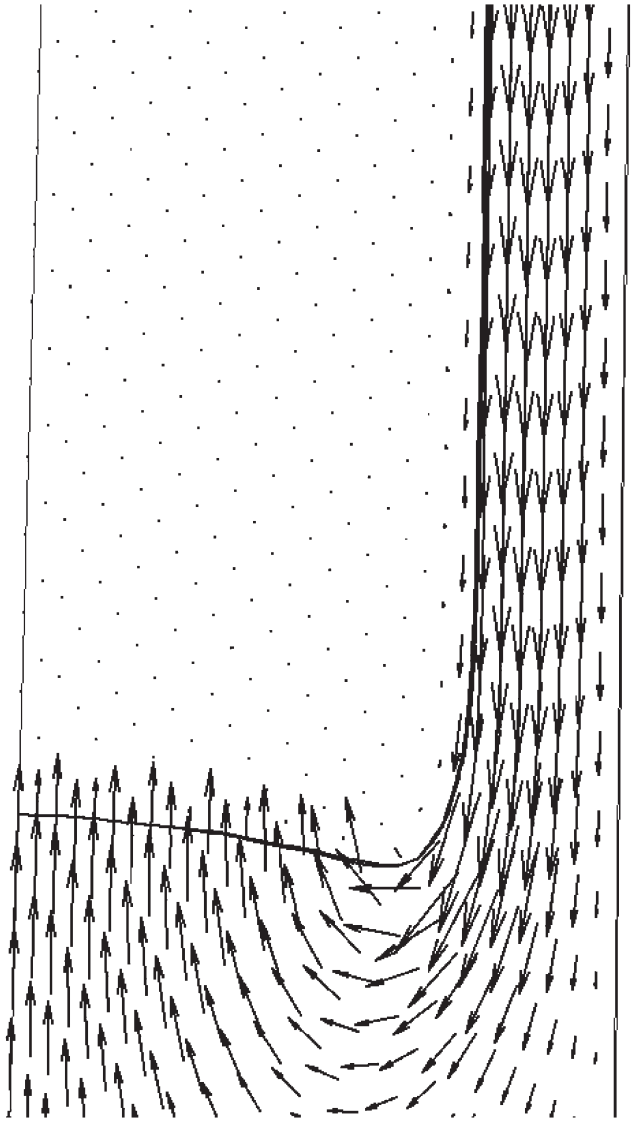

Figure 10. The velocity field in the wake region of the Taylor bubble. (Vectors are shown at only one-fifth of the computational nodes for clarity.)

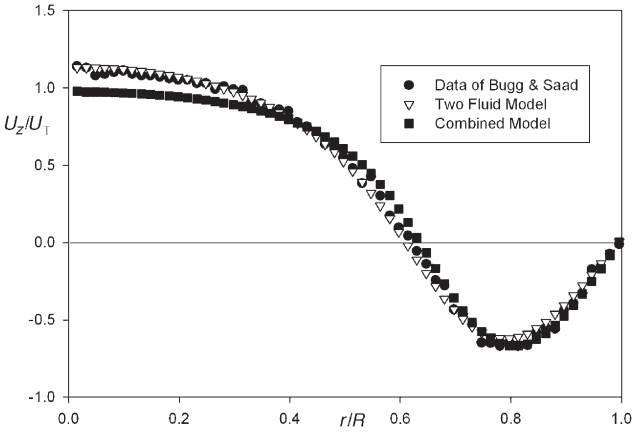

Figure 11. The axial velocity profile in the wake of the bubble.

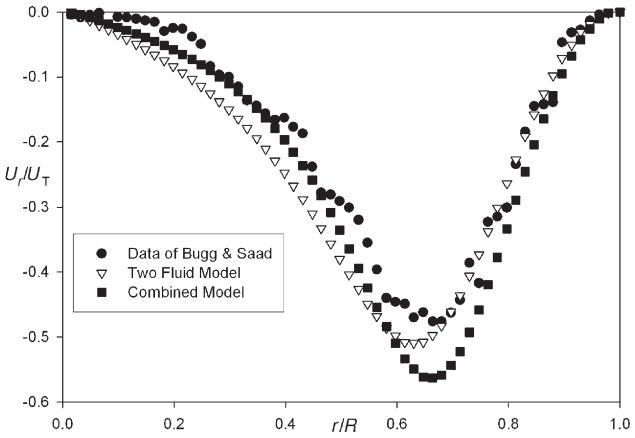

Figure 12. The radial velocity profile in the wake of the bubble.

APPLICATION TO TUBULAR MEMBRANE SYSTEMS

Simulations were performed using the above model to investigate two specific issues of relevance to tubular membrane systems. Firstly, we investigated whether extraction of fluid at the membrane surface changes the flow behaviour in any way. Secondly, we investigated the wall shear stress distribution in order to determine the shape of the profile and the behaviour in the bubble wake.

Simulation Conditions

We used the same geometry and fluid properties as described above in these simulations, and therefore the *Eo* and *Mo* numbers are the same as those reported earlier. The only difference was that fluid was injected at the base of the tube and was allowed to exit at the top. Simulations were performed for inlet liquid velocities of 0.06 and 0.1 m s^{-1}, corresponding to inlet Reynolds numbers of 114 and 190, respectively. In addition, extraction from the wall was varied between 0 and 20% for a pipe length of 16 pipe diameters. The pipe was oriented vertically so that the bubble rose due to buoyancy in the co-flowing

liquid, exactly as in a real membrane system. Simulations were continued until a steady rise velocity was obtained.

Results

Axial shear stress profiles for the case of a liquid velocity of 0.06 m s^{-1} are shown in Figure 13. The shear stress is plotted against axial distance, with the profiles aligned so that the bubble is in the same physical location in each case. The figure shows the expected shear stress profile, with increased shear stress in the film region, a flat profile in the region of fully developed flow in the film and abrupt changes at the bubble nose and in the wake region. There is almost no effect of fluid extraction observable in the figure.

A detailed view of the wake region is shown in Figure 14. The figure shows that as the fluid is extracted there is a reduction in the magnitude of the shear stress due to the reduced flow, as expected. It also shows that there are small amplitude oscillations, which are resolved by the simulations. Examination of the velocity field shows that these are located in the region where the flow changes abruptly from vertically upwards in the pipe to descending in the film. Results for a simulation at a higher inlet liquid velocity of 0.1 m s^{-1} exhibited the same behaviour as at the lower liquid velocity and are therefore not shown here.

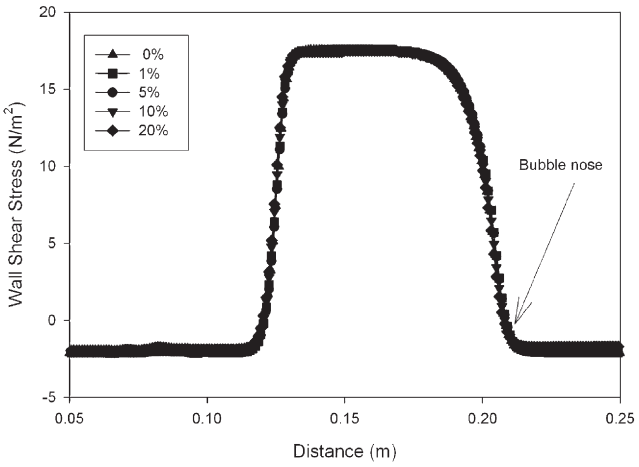

Figure 13. The wall shear stress distribution along the pipe for a liquid flow rate of 0.06 m s^{-1} showing the very minor effect of liquid extraction.

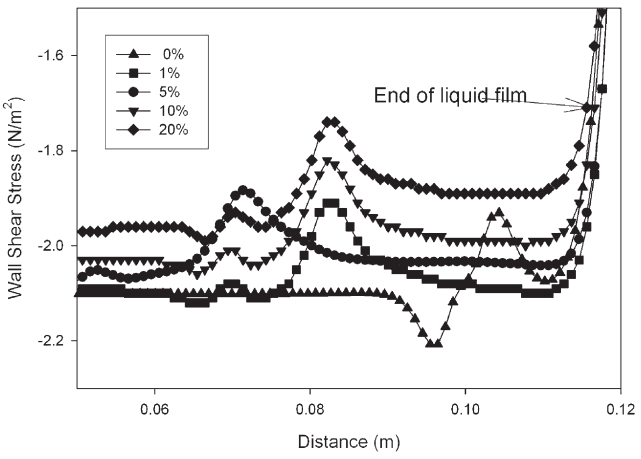

Figure 14. Details of the wall shear stress profile in the wake region for the liquid velocity of 0.06 m s^{-1} case and various extraction rates. The smooth nature of the stress profiles is evident.

Discussions

The above results show that there is almost no influence of extraction on wall shear stress profiles and that as far as flux enhancements effects caused by the rising bubble are concerned, allowing for fluid extraction is not warranted. This would apply even more so to cases where fouling has occurred, as the fluxes would be even lower.

A feature of the current results that is noteworthy is the very smooth variation of the shear stress profiles, even in the wake region. They suggest that a simple 'top-hat' shaped shear stress function could be used in simplified membrane models to simulate the effect of the bubble. This is in stark contrast with the results presented by Taha and Cui (2002), who showed very high frequency oscillations with an amplitude of 20–50% of the peak shear stress. Their simulations were performed using similar (but not the same) numerical methods to us. In addition, their flows were for higher Reynolds numbers, in the range of 1600–10,000, than those studied here (Reynolds numbers up to 200). A key difference in the simulation procedure was that they treated the simulations as being turbulent and used the RNG $k-\varepsilon$ model to close the equations. This is a high Reynolds number turbulence model and is certainly not applicable at low Reynolds numbers. Their Reynolds number of 1600 case, which shows the very high amplitude, high frequency oscillations in the wake, would be laminar and the higher Reynolds number flows would be transitional, without a fully developed log-law region near the wall, as required by high Reynolds number turbulence models. Therefore it seems most likely that their oscillations were numerical rather than physical in origin.

Note that the results presented here are restricted to laminar flow. The simulations presented are very costly because of the need to use fine meshes and small time steps to obtain accurate and stable solutions. Their extension to higher Reynolds numbers is not straightforward, as the Reynolds numbers are not high enough to assume fully turbulent flow with equilibrium log law layers at the wall. This conclusion is valid not only for the flow in the tube but is even more strongly the case in the film around the bubble.

CONCLUSIONS

Results for the simulation of laminar flow of a Taylor bubble in a tube with and without fluid extraction at the wall have been presented. A comprehensive validation exercise has been performed to validate a general purpose CFD code. These simulations are not limited to the determination of the steady-state bubble shape, as in most previous studies, but follow the transient evolution of the bubble. Three different models have been tested, namely a VOF model, a two-fluid Eulerian model with a constant disperse phase bubble size and a combined model that uses a solution adapted disperse phase length-scale to obtain the best features of both models. The limitation of

the validity of the VOF model in the wake region, due to excessive mixing, was an unexpected finding of this study, that necessitated the use of the two fluid model to overcome this numerical problem. In the two fluid model, the mixing can be avoided by defining the gas phase as a disperse phase with a large bubble size, so that any numerical mixing is undone by gravitational segregation.

In all regions around the Taylor bubble, the predicted velocity profiles show good agreement with the experimental data. The bubble shape and terminal velocity are well predicted by the numerical models. Although the velocity profile in the wake region could not be obtained with the VOF model, this model produced good results in all other regions around the bubble. Using the combined model reduced the excessive thickness of the gas–liquid interface that was present in the two-fluid model that used a constant dispersed phase length-scale. The combined model produced a bubble with a sharp interface and gave the best results of the models investigated.

This exercise also highlighted the need for extremely fine computational meshes if this type of flow is to be properly resolved. There are very significant velocity gradients around the bubble nose and tail, with velocity values changing by 25% over distances of only 0.5 mm. This has implications not only for numerical modelling, where coarse grids are often used to cut the very high computational costs, but also for comparison with experimental data, where some uncertainty as to the exact location of the bubble interface is always present.

The presented results also show that there is no significant effect of the fluid extraction on the wall shear stress for conditions relevant to tubular membranes. Moreover, we show that there are no significant oscillations in the wall shear stress in the wake regions for the cases studied and that the shear stress change can be well represented by a 'top-hat' profile. This conclusion is valid for a much higher range of extraction rates than used in commercial membrane systems and applies to systems with and without fouling.

REFERENCES

Bellara, S.R., Cui, Z.F. and Pepper, D.S., 1996, Gas sparging to enhancement permeate flux in ultrafiltration using hollow fibre membranes, *J Membr Sci*, 121: 175.

Brackbill, J.U., Kothe, D.B. and Zemach, C., 1992, A continuum method for modeling surface tension, *J Comput Phys*, 100: 335.

Bugg, J.D. and Saad, G.A., 2002, The velocity field around a Taylor bubble rising in a stagnant viscous fluid: numerical and experimental results, *Int J Multiphase Flow*, 28: 791.

Bugg, J.D., Mack, K. and Rezkallah, K.S., 1998, A numerical model of Taylor bubbles rising through stagnant liquids in vertical pipes, *Int J Multiphase Flow*, 24: 271.

Cabassud, C., Laborie, S. and Laine, J.M., 1997, How slug flow can improve ultrafiltration flux in organic hollow fibres, *J Membr Sci*, 128: 93.

Cabassud, C., Laborie, S., Durand-Bourlier, L. and Laine, J.M., 2001, Air sparging in ultrafiltration hollow fibres: relationship between flux enhancement, cake characteristic and hydrodynamic parameters, *J Membr Sci*, 181: 57.

Clarke, A. and Issa, R.I., 1997, A numerical model of slug flow in vertical tubes, *Comput Fluids*, 26: 395.

Cui, Z.F. and Taha, T., 2003, Enhancement of ultrafiltration using gas sparging: a comparison of different membranes modules, *J Chem Technol Biotechnol*, 78: 249.

Cui, Z.F. and Wright, K.I.T., 1996, Flux enhancement with gas sparging in downwards cross-flow ultrafiltration: performance and mechanism, *J Membr Sci* 117: 109.

Cui, Z.F., Chang, S. and Fane, A.G., 2003, The use of gas bubbling to enhance membrane processes—a review, *J Membr Sci*, 221: 1.

Ducom, G., Puech, F.P. and Cabassud, C., 2002, Air sparging with flat sheet nanofiltration: a link between wall shear stresses and flux enhancement, *Desalination*, 145: 97.

Fabre, J. and Liné, A., 1992, Modeling of two-phase slug flow, *A. Rev Fluid Mech*, 24: 21.

Ghosh, R. and Cui, Z.F., 1999, Mass transfer in gas-sparged ultrafiltration: upward slug flow in tubular membranes, *J Membr Sci*, 162: 91.

Harvie, D.J.E. and Fletcher, D.F., 2000, A new volume of fluid advection algorithm: The stream scheme. *J Comput Phys*, 162: 1.

Hirt, C.W. and Nichols, B.D., 1981, Volume of fluid (VOF) method for the dynamics of free boundaries, *J Comput Phys*, 39: 201.

Howell, J.A., Field, R.W., Mackley M.R. and Wang, Y., 1992, The simulation of particle advection in a porous baffled channel subject to pulsatile flow, Preprints, *IChemE Research Event* (IChemE, Rugby, UK), p. 386.

Issa, R.I. and Ubbink, O., 1999, Numerical prediction of Taylor bubble dynamics using a new interface capturing technique, in *Proceedings of 3rd ASME/JSME Joint Fluids Engineering Conference*, 18–23 July, 1999, San Francisco, CA.

Kawaji, M., DeJesus, J.M. and Tudose, G., 1997, Investigation of flow structures in vertical slug flow, *Nucl Eng Des*, 175: 37.

Lee, C.K., Chang, W.G. and Ju, Y.H., 1993, Air slugs entrapped cross-flow filtration of bacterial suspensions, *Biotechnol Bioeng*, 41: 525.

Mao, Z.-S., and Dukler, A.E., 1991, The motion of Taylor bubbles in vertical tubes II. Experimental data and simulations for laminar and turbulent flow, *Chem Eng Sci*, 46: 2055.

Mercier, M., Fonade, C. and Lafforgue-Delorme, C., 1997, How slug flow can enhance the ultrafiltration flux in mineral tubular membranes, *J Membr Sci*, 128: 103.

Mercier, M., Maranges, C., Fonade, C. and Lafforgue-Delorme, C., 1998, Yeast suspension filtration: flux enhancement using an upward gas/liquid slug flow—application to continuous alcoholic fermentation with cell recycle, *Biotechnol Bioeng*, 58: 47.

Mercier-Bonin, M., Maranges, C., Lafforgue, C. and Fonade, C., 2000, Hydrodynamics of slug flow applied to cross-flow filtration in narrow tubes, *AIChE J*, 46: 476.

Taha, T. and Cui, Z.F., 2002, CFD modeling of gas-sparged ultrafiltration in tubular membranes, *J Membr Sci*, 210: 13.

Taitel, Y., Shoham, O. and Brill, J.P., 1989, Simplified transient solutions and simulations of two-phase flow in pipelines, *Chem Eng Sci*, 44: 1353.

Tomiyama, A., Zun, I., Sou, A. and Sakaguchi, T. 1993 Numerical analysis of bubble motion with the VOF method, *Nucl Eng Des*, 141: 69.

Vera, L., Villarroel, R., Delgado, S. and Elmaleh, S., 2000, Enhancing microfiltration through an inorganic tubular membrane by gas sparging, *J Membr Sci*, 165: 47.

Wang, Y., Howell, J.A., Field, R.W. and Wu, D., 1994, Simulation of cross-flow filtration for baffled tubular channels and pulsatile flow, *J Membr Sci*, 95: 243.

White, E.R. and Beardmore, R.H., 1962, The velocity of rise of single cylindrical air bubbles through liquids in vertical tubes, *Chem Eng Sci*, 17: 351.

ACKNOWLEDGEMENTS

The authors would like to thank Professor J.D. Bugg of Saskatchewan University for providing the experimental data, Phil Zwart of ANSYS CFX for useful discussions and AusAID for providing a scholarship to Vincent Ndinisa.

The manuscript was received 5 November 2003 and accepted for publication after revision 1 September 2004.